Acta Oceanol. Sin., 2022, Vol. 41, No. 2, P. 139–146
https://doi.org/10.1007/s13131-021-1837-8
http://www.aosocean.com
E-mail: ocean2@hyxb.org.cn

Turning depths of internal tides in the South China Sea inferred from profile data

Kun Liu[1], Lianglong Da[1, 2*], Wuhong Guo[1, 2], Chenglong Liu[1], Junchuan Sun[1, 3]

[1] Pilot National Laboratory for Marine Science and Technology (Qingdao), Qingdao 266237, China

[2] PLA Navy Submarine Academy, Qingdao 266041, China

[3] Key Laboratory of Marine Science and Numerical Modeling, First Institute of Oceanography, Ministry of Natural Resources, Qingdao 266061, China

Received 28 October 2020; accepted 29 March 2021

Abstract

Theoretically, propagating internal tides in the ocean may reflect at turning depths, where buoyancy frequencies equal tidal frequencies, before colliding with the air-sea interface or rugged bottom topography. Globally, the internal tide lower turning depths (ITLTDs) in the open ocean have been mapped; however, knowledge of the presence of ITLTDs in the South China Sea (SCS) is lacking. In this study, 2 125 high-quality temperature-salinity profiles (including 58 deep-sea hydrographic measurements with observational depths exceeding 3 000 m) are collected and analyzed to investigate the existence of ITLTDs in the SCS. Furthermore, the concept of the upper turning depth is first introduced in the context of internal tides, and internal tide upper turning depths (ITUTDs) are also investigated. ITLTDs are found to exist at several abyssal stations; these stations are distributed mostly in the southern part of the SCS basin, possibly due to the greater water depths there. Fewer locations show the presence of ITLTDs for K_1 versus M_2 tidal frequencies because of the lower tidal frequency. The distance between ITLTDs and the seafloor ranged from 270 m to more than 1 200 m, implying the possible existence of multiple internal wave evanescent regions in the abyssal bottom. ITUTDs of tens of meters are ubiquitous in the SCS; stations with the presence of ITUTDs are located mainly in the northeastern SCS due to the intensive observations there. However, the calculated ITUTDs have large uncertainties; they are sensitive to the selected bin values. The horizontal propagation directions of internal tides in the SCS change dramatically, and as a result, the estimated turning depths under the full Coriolis force definition are different compared to that under the traditional approximation.

Key words: turning depth, internal tide, buoyancy frequency, South China Sea

Citation: Liu Kun, Da Lianglong, Guo Wuhong, Liu Chenglong, Sun Junchuan. 2022. Turning depths of internal tides in the South China Sea inferred from profile data. Acta Oceanologica Sinica, 41(2): 139–146, doi: 10.1007/s13131-021-1837-8

1 Introduction

Internal tides are ubiquitous in the ocean and have dual impacts on human maritime activities. First, the breaking of internal tides is regarded as one of the major catalysts of ocean mixing, which is crucial for large-scale ocean circulation (Munk and Wunsch, 1998). Internal tidal-induced upwelling can pump nutrients upward to the euphotic layer; this surface nutrient enrichment can in turn increase fishing yields (Jan and Chen, 2009). Second, the steepening of internal tides can induce large-amplitude internal solitary waves, which are key environmental factors in the design of offshore oil and gas engineering projects. Internal waves are considered to be second only to typhoons in terms of disaster potential due to the enormous threat they pose to undersea equipment (Fang and Duan, 2014).

The propagation of internal tides in the ocean is significantly affected by the inhomogeneous hydrological environment (Gerkema et al., 2004). In linear theory, freely propagating internal waves have a lower frequency limit of the local inertial frequency and a higher frequency limit of the buoyancy frequency ($f < \omega < N$). In view of this theoretical basis and the fact that buoyancy frequencies are generally exponentially dampened with depth in the abyssal sea, Munk (1981) first proposed the possible existence of internal tide turning depths, where the local buoyancy frequency matches the tidal frequency. The presence of turning depths can impact the pathways and energy losses of internal tides during propagation by reflecting or refracting internal tidal beams at the turning interface and preventing internal tides from colliding with rugged bottom topographies. Numerical and experimental studies have suggested that internal tidal beams behave remarkably differently according to the presence or absence of turning depths (Paoletti and Swinney, 2012). Moreover, the existence of turning depths may affect the generation of internal tides beneath them (Paoletti et al., 2014).

The identification of internal tide turning depths requires hydrographic observations of the abyssal ocean. Based on World Ocean Circulation Experiment data, King et al. (2012) mapped

Foundation item: The National Natural Science Foundation of China under contract Nos 41906005, 41149907 and 41706033; the National Basic Research Program of China under contract No. 2019-JCJQ-ZD-149-00; the Open Fund of the Laboratory for Regional Oceanography and Numerical Modeling, Pilot National Laboratory for Marine Science and Technology (Qingdao) under contract No. 2019A05.

*Corresponding author, E-mail: da_lianglong@126.com

the global spatial distribution of M_2 internal tide turning depths and suggested that turning depths are common in oceans with depths greater than 4 000 m. However, available deep-sea hydrographic observations are concentrated mainly in the open ocean. The South China Sea (SCS) is a marginal sea in the western Pacific, in which internal tidal processes are very active compared to the world oceans (Niwa and Hibiya, 2011). The central deep basin of the SCS features an average depth of more than 3 000 m. Thus, the existence of turning depths is highly possible. However, to our knowledge, internal tide turning depths in the SCS have not yet been reported. A broad understanding of turning depths in the SCS may deepen our insight into the generation, propagation and dissipation processes of internal tides.

The existence of internal tide turning depths in the SCS is still unknown mainly due to very limited deep-sea sampling. Despite the large number of historical hydrographic profiles in the SCS, deep-sea hydrographic profiles are extremely rare. For example, there are more than 2 000 World Ocean Database 2018 (WOD18) temperature and salinity profiles in the SCS with observational depths greater than 1 000 m, but that number decreases to 15 profiles when the observational depth is extended to greater than 3 000 m. In March of 2012, with the support of the Oceanographic Research Vessel Sharing Plan of the National Natural Science Foundation of China (NSFC), the Ocean University of China obtained 32 deep-sea hydrographic measurements (>3 000 m) with a spatial coverage of nearly the entire central deep basin (Fig. 1). These modern high vertical resolution and high-quality data together with historically accumulated data provide an opportunity to explore the existence of internal tide turning depths in the SCS.

Moreover, strictly speaking, all the abovementioned internal tide turning depths refer to internal tide lower turning depths (ITLTDs), which are close to the bottom. In fact, the buoyancy frequencies within the surface mixed layer are also very small and may be less than the tidal frequencies. However, the concept of upper turning depths has rarely been mentioned in the context of internal tides; it is more widely used in the field of acoustical oceanography (Dushaw and Sagen, 2017). The presence of internal tide upper turning depths (ITUTDs) could also impact the propagation of internal waves. For example, Liang et al. (2019) attained a better correlation between numerical predictions and observations on the arrival times of incident internal waves when internal waves reflected at the subsurface at approximately 50 m.

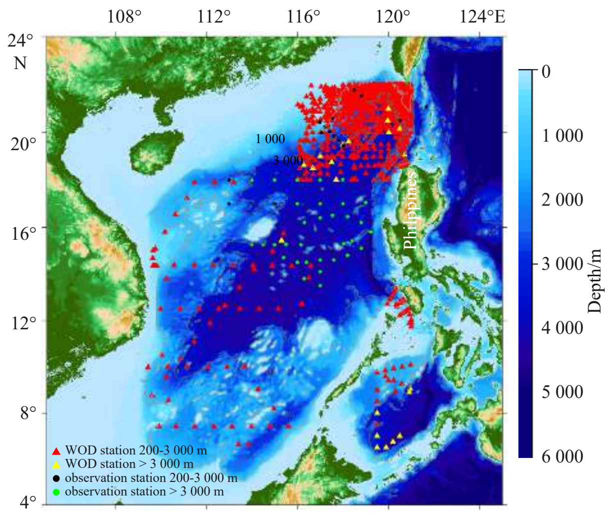

Fig. 1. Topography and observation stations in the South China Sea. The triangles and the dots represent the *in situ* observation stations of the WOD18 and 2012 NSFC cruises, respectively. The yellow triangles and green dots denote profiles with observational depths greater than 3 000 m, which are used for internal tide lower turning depth identification. The red triangles and black dots denote profiles with observational depths greater than 200 m but less than 3 000 m; all the available profiles are used for internal tide upper turning depth identification. The background gray contours indicate the 1 000 m and 3 000 m isobaths, respectively.

This study explored the existence of ITUTDs and ITLTDs in the SCS based on new ocean observations as well as historical hydrographic data. The M_2 and K_1 tidal constituents were chosen to represent the most important semidiurnal and diurnal internal tides, respectively. The existence of ITUTDs and ITLTDs is confirmed in the SCS and turning depths are found to distribute over a broad spatial area. In Section 2, the data and analysis methods are described. In Section 3, the observational evidence for the existence of ITUTDs and ITLTDs in the SCS is provided. The spatial distribution of turning depths is mapped based on the available data. Furthermore, estimating the turning depth under the full influence of the Coriolis force is discussed. The main results of this study are summarized in Section 4.

2 Data and methodology

2.1 *NSFC observation*

To investigate the existence of internal tide turning depths in the SCS, the hydrographic data collected by the open cruise of the NSFC in the SCS in March of 2012 is analyzed. During the cruise, a total of 48 sets of hydrographic profiles were obtained, and 35 of these profiles have observational depths exceeding 3 000 m (see locations in Fig. 1). The observational depths of all the profiles exceed 200 m. The extensive horizontal spatial coverage and vertical depth range of the conductivity-temperature-depth (CTD) profiles allow an accurate analysis of the existence of internal tide turning depths in the SCS. These CTD profiles were recorded by the Seabird SBE-911 and have a temperature accuracy of 1 mK and a conductivity accuracy of 0.3 mS per meter. The vertical resolution of the data is 1×10^4 Pa.

2.2 *WOD18 data*

To supplement the NSFC hydrographic measurements and uncover more observational evidence of internal tide turning depths in the SCS, WOD18 data, which represent the most comprehensive collection of ocean hydrographic data currently available, were also analyzed. The WOD18 data include quality-controlled observational data for more than 15.7 million temperature profiles and 8.5 million salinity profiles (Boyer et al., 2018) and are available from the National Oceanographic Data Center (https://www.nodc.noaa.gov/OC5/WOD/pr_wod.html). Given the main focus of this study, only WOD18 high-resolution CTD hydrographic profiles within 4°–24°N and 105°–121°E with the deepest measurement exceeding 200 m are considered. After screening, a total of 2 077 WOD18 profiles from the years 1773 to 2019 met these requirements, within which 23 profiles have observational depths greater than 3 000 m (15 deep-sea measurements in the SCS and 8 deep-sea measurements in the Sulu Sea). All the analyzed WOD18 profiles are at the observation depths.

The WOD18 stations cover nearly the entire SCS (Fig. 1); they have better spatial coverage than the NSFC observations due to the longer period of data accumulation, but the NSFC observations have more deep-sea hydrographic measurements. To obtain more abyssal data, gridded data products such as the US Navy Generalized Digital Environment Model (GDEM) is also analyzed, which are available at 78 standard depths (ranging from the surface down to 6 600 m; Carnes, 2009). However, temperature-salinity plots indicate that the abyssal GDEM data show obvious data interpolation (not shown here). Calculating the buoyancy frequencies in weakly stable waters utilizing original profiles is more reliable than using a gridded dataset. The final dataset used in this study consisted of 48 NSFC and 2 077 WOD18 temperature/salinity profiles, with 58 profiles having observational depths exceeding 3 000 m. Using this dataset, this study aimed to obtain a spatial map of internal tide turning depths in the SCS.

2.3 *Computation of the squared buoyancy frequency*

Quality control was applied to the raw temperature and salinity profiles from each station; duplicate profiles and abnormal values were removed. The original hydrographic data have a "wiggly" nature due to the observation accuracy of the instruments (Fig. 2). For instance, in the WOD18 data, the accuracies of the temperature and conductivity sensors are 1–5 mK and 0.3–2 mS per meter, respectively (Boyer et al., 2018). Fluctuations in temperature and salinity data can lead to large fluctuations in the buoyancy frequency. Therefore, the raw hydrographic temperature and salinity data (T_{raw} and S_{raw}, respectively) were smoothed before calculating the buoyancy frequency. The entire water column was vertically divided into several bins with a constant depth, and T_{raw} and S_{raw} in each bin were averaged (Fig. 2).

The ocean stability is weak near the surface and at great depths; thus, the determination of turning depths requires the most precise buoyancy frequency calculation possible. Van Haren and Millot (2006) sought to determine the buoyancy frequency in weakly stable waters and concluded that CTD observations can be used to estimate water stability with an error of ~0.8 f (with an average over 1×10^6 Pa, where f is the inertial frequency). In the SCS (~10°–20°N), 0.8 f ranges from 2.53×10^{-5} rad/s to 4.98×10^{-5} rad/s, which is less than the tidal frequency (1.41×10^{-4} rad/s and 7.29×10^{-5} rad/s for semidiurnal and diurnal frequencies, respectively); thus, the observed temperature and salinity profiles of the CTD data can indicate the existence of internal tide turning depths in the SCS.

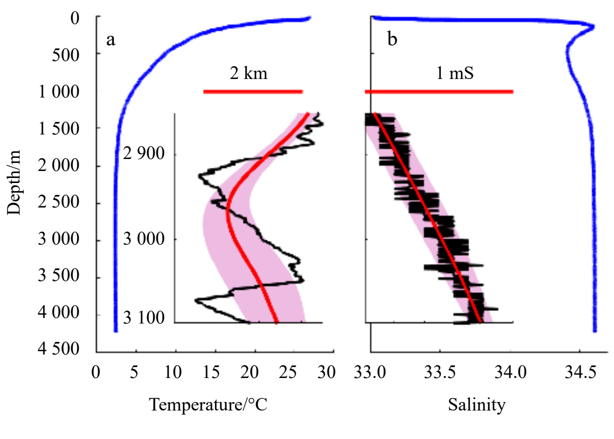

Fig. 2. Profiles of temperature (a) and salinity (b) (blue lines) at a WOD18 station (15.42°N, 115.31°E). The original (black lines) and smoothed (red lines, bin of 100 m) profiles at the a depth between 2 850 m and 3 100 m are amplified and shown in the insets; the pink patches denote the standard deviation calculated by the Monte Carlo method.

The buoyancy frequency indicates the natural frequency of vertically oscillating fluid parcels in the continuously stratified water and can be derived in terms of the vertical gradients of potential temperature T, and absolute salinity S_{a}, such that

$$N^2(z) = g\left(\alpha\frac{\partial T}{\partial z} - \beta\frac{\partial S_{\mathrm{a}}}{\partial z}\right), \tag{1}$$

where g is the gravitational acceleration, and α and β are the depth-dependent thermal expansion coefficient and the saline contraction coefficient, respectively. $N^2(z)$ is not calculated by the vertical potential density gradients because the density of water is not a directly observed variable, and calculating the buoyancy frequency utilizing the potential density expression may underestimate the strength of the stability (Lynn and Reid, 1968). In this study, the Gibbs SeaWater toolbox was adopted to calculate the buoyancy frequency (http://www.teos-10.org). This toolbox is based on the new thermodynamic seawater equation TEOS-10, and the ocean state is depicted more accurately by considering the spatially dependent S_{a} (Li et al., 2013).

As suggested by King et al. (2012), the squared buoyancy frequency ($N^2(z)$), rather than the buoyancy frequency was calculated to determine the existence of a turning depth because the squared version was used in the internal wave governing equation. The squared buoyancy frequency can also be negative, indicating convective instability. Vertical profiles of the bin-averaged squared buoyancy frequency ($N^2_{\mathrm{bin}}(z)$) and the associated standard deviation ($SD_{N^2_{\mathrm{bin}}}$) were obtained by utilizing a Monte Carlo method following the calculation process of King et al. (2012). First, the bin-averaged temperature and salinity (T_{bin} and S_{bin}) were spline-fitted to the entire water column, and the standard deviations of temperature and salinity ($SD_{T_{\mathrm{bin}}}$ and $SD_{S_{\mathrm{bin}}}$) and the number of samples in each bin (M_{bin}) were obtained. Then, a set of synthetic data samples was devised based on sample functions (2) and (3); the number of samples was set to 500 following King et al. (2012).

$$T_{\mathrm{sample}} = T_{\mathrm{bin}} + \mathrm{noise} \times SD_{T_{\mathrm{bin}}}/\sqrt{M_{\mathrm{bin}}}, \tag{2}$$

$$S_{\mathrm{sample}} = S_{\mathrm{bin}} + \mathrm{noise} \times SD_{S_{\mathrm{bin}}}/\sqrt{M_{\mathrm{bin}}}. \tag{3}$$

Finally, $N^2(z)$ was calculated based on the synthetic data, and $N^2_{\mathrm{bin}}(z)$ and $SD_{N^2_{\mathrm{bin}}}$ were obtained. Generally, $N^2(z)$ is large at the main pycnocline (a gradual interface separating two fluids of different densities) and decreases exponentially from the pycnocline to both the surface and bottom boundaries. In the SCS, the main pycnocline depth is approximately 120 m, which was obtained from satellite altimetry estimation (Chen et al., 2017). Thus, the distance from the main pycnocline to the ITLTD is far more than that to the ITUTD, and the bin widths are different for ITLTD and ITUTD identification. The sensitivity of the calculated results to different bin widths is shown in Section 3.1.

3 Results and discussion

3.1 *Examples of the existence of turning depths in the SCS based on observational data*

The buoyancy frequency commonly peaks at the depth of the pycnocline and decreases from the pycnocline to both the surface and bottom boundaries. The existence of ITLTDs was first investigated. An example of the deep-sea $N^2(z)$ calculated at one station (14.1°N, 117.0°E) is shown in Fig. 3; obviously, the depth-dependent $N^2(z)$ crosses the M_2 and K_1 tidal frequencies at depths of approximately 3 660 m and 3 870 m, respectively. The K_1 ITLTDs are greater than those of M_2 at the same locations due to the lower tidal frequency. The distance between the ITLTDs and the seafloor is approximately 380–590 m, which corresponds to a thick, deep, "homogeneous" layer of weak stability. The calculated ITLTDs are basically consistent under different bin values of 50 m, 100 m and 200 m (Fig. 3). These findings confirm that ITLTDs exist in deep marginal seas in addition to the abyssal open ocean.

Notably, an optimum bin size must be selected to calculate the turning depth. The squared buoyancy frequency profiles may swing drastically due to small bin values (Fig. 3a), which could lead to an incorrect supposition of the existence of several turning depths. Buoyancy frequency profiles become smoother with a larger bin size and are more representative of the vertical stratification structure. However, at the other extreme, buoyancy frequency profiles may not be able to cross tidal frequencies due to large bin sizes because large bin values correspond to a reduction in the number of deep samplings (Fig. 3c). Thus, in a subsequent analysis, a 100 m bin size as suggested by King et al. (2012) was selected to avoid multiple crossings between the squared buoyancy frequency profile and the tidal frequencies and to simultaneously ensure the reliability of the calculated ITLTD. However, the 100 m bin size could also result in multiple crossings, and the ITLTDs at these stations were obtained by calculating the mean of the crossing depths.

In contrast to the very limited abyssal observations, a stronger data foundation was available for the investigation of the ITUTDs. Figure 4a shows a sample of upper ocean $N^2(z)$ values calculated at one station (20.25°N, 117.21°E), in which the thickness of the upper mixed layer (within which the density discrepancies are less than 0.01 kg/m³) is approximately 25 m. A closer view of the vertical distribution of $N^2(z)$ values within the mixed layer (Fig. 4b) shows that the water stability in the upper mixed layer is very weak, and the calculated $N^2(z)$ profiles with small bin values cross the tidal frequencies many times. Similar to the ITLTD calculation, the bin values were increased to smooth the $N^2(z)$ profile. Considering that the pycnocline is much closer to the ocean surface than the ocean bottom, $N^2(z)$ decreases upward from the

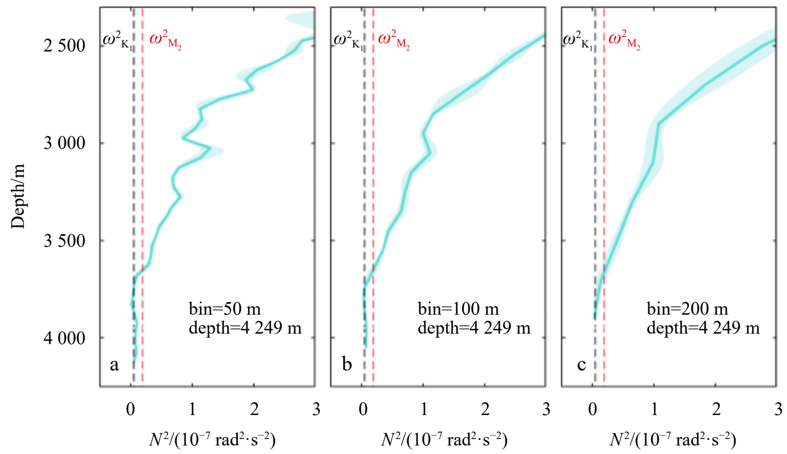

Fig. 3. Squared buoyancy frequency profiles calculated under different bin values 50 m (a), 100 m (b), and 200 m (c) at the station located at 14.1°N and 117.0°E. The cyan lines and patches indicate the bin-averaged squared buoyancy frequency and associated standard deviation, respectively. The black and red dashed lines indicate the K_1 and M_2 tidal frequencies, respectively.

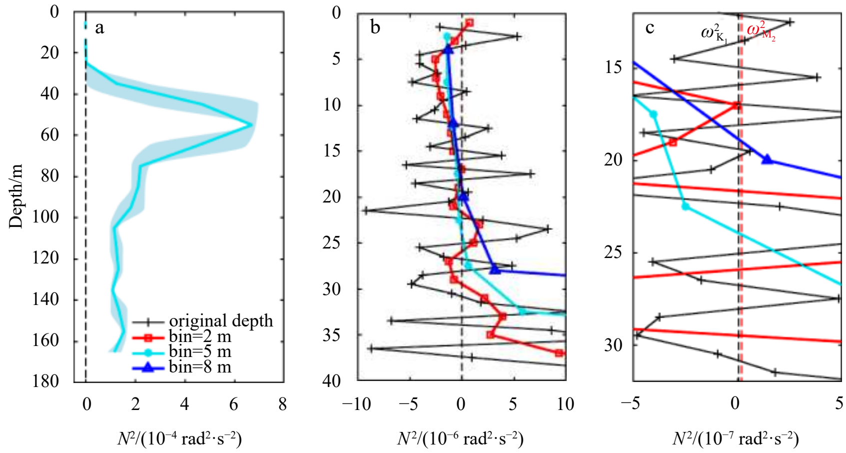

Fig. 4. The squared buoyancy frequency profiles calculated with a 5 m bin at the station located at 20.25°N and 117.21°E (a), and amplified views of the squared buoyancy frequency profiles at the observational depth and with different bin values (2 m, 5 m and 8 m) in the upper ocean (b, c). In a, the cyan lines and patches indicate the bin-averaged squared buoyancy frequency and associated standard deviation, respectively. In b and c , the black and red dashed lines indicate the K_1 and M_2 tidal frequencies, respectively. Note that the horizontal coordinates are different among the subplots.

maximum value at the pycnocline to tidal frequencies within a very short distance if ITUTDs exist; the bin values in the ITUTD calculation are much less than those in the ITLTD calculation. When the bin sizes are greater than 5 m, the $N^2(z)$ profiles are smooth and are still able to cross tidal frequencies, and this result confirms the existence of ITUTDs and indicates the fact that propagating internal tides can reflect at the subsurface. However, the estimated ITUTDs are different under different bin values and it is difficult to determine an optimal bin value convincingly. One possible reason is that, in contrast to the relatively quiet abyssal ocean, the upper boundary is influenced by winds and surface buoyancy fluxes, and the $N^2(z)$ profiles may not exhibit a monotonous decreasing trend from the pycnocline to the sea surface. The coexistence of multiple ITUTDs at one single profile may be closer to the real oceanic scenario. Thus, ITUTD estimations include more uncertainty than ITLTD estimations. In the following section, a 5 m bin size is selected to obtain a reference value for ITUTDs in the SCS. If there are multiple crossings between the $N^2(z)$ profiles and the tidal frequencies, ITUTDs are determined by calculating the mean of the crossing depths.

3.2 *Spatial distribution of turning depths in the SCS*

Based on the $N^2(z)$ profiles calculated from both the NSFC and WOD18 observations, a comprehensive picture of turning depths in the SCS can be obtained. Among the 58 abyssal ocean observations, ITLTDs exist at 16 (and 12) stations for M_2 (and K_1) internal tides (Figs 5 and 6). At certain stations, ITLTDs may also exist but are not detected because of the incomplete observational coverage of the full water depth. Because K_1 internal tides have lower frequencies, in rare cases, the minimum $N^2(z)$ may cross only M_2 tidal frequencies but fail to reach K_1 tidal frequencies. Horizontally, ITLTDs are distributed over a wide spatial area in the SCS (Figs 5a and 6a) but are concentrated mainly in the southern part of the deep basin. This north–south asymmetry may result from the fact that the water is deeper in the south. The maximum ITLTD exceeds 4 500 m in the vicinity of the Manila Trench. ITLTDs also exist in the Sulu Sea according to limited observations. Vertically, the distances between ITLTDs and the seafloor range from 270 m to more than 1 200 m (Figs 5b and 6b), which implies the existence of a broad evanescent region at multiple locations at the bottom. The maximal distance between the turning points and the seafloor occurs near the southern boundary of the deep basin. The residence time of the deep water in the SCS deep basin is approximately 30–100 years (Broecker et al., 1986; Qu et al., 2006), and $N^2(z)$ profiles for depths greater than 1 000 m can exhibit very limited variations over several years (King et al., 2012). Therefore, the map presented in this study may shed light on the basic spatial features of ITLTDs in the SCS. More high-quality deep-sea hydrographic measurements are needed in the future to complete the details on the map.

Figure 7a shows the spatial distribution of M_2 ITUTDs in the SCS. At each station, the calculated ITUTDs are nearly the same for M_2 and K_1 frequencies (Fig. 4c); therefore, the map of K_1 ITUTDs is not shown here. Among the 2 125 ocean observations, upper turning depths exist at 210 stations for both M_2 and K_1 internal tides. Most of the stations with the presence of ITUTDs are located in the northeastern SCS, where the most intensive observations are located. The maximum calculated ITUTD is 93.7 m; this indicates that the internal wave evanescent region near the surface is not as spacious as that in the abyssal bottom. Moreover, the calculated ITUTDs are different among neighboring stations, which may be caused by the difference in observation times. In contrast to the relatively quiet abyssal ocean, the upper ocean is stirred by winds and surface buoyancy fluxes. Thus, ITUTDs can be highly variable both temporally and spatially. To quantify the uncertainties of the calculated ITUTDs, the standard deviations of the obtained ITUTDs under different bin values of 2–8 m were calculated (Fig. 7b). Note that the standard deviations were calculated only at stations where ITUTDs could be detected under all of the abovementioned bin values. The standard deviations are generally less than 10 m at most stations; at a few stations, the standard deviations can exceed 15 m. Compared to the ITUTDs in the 5 m bin, the percentage of uncertainty ranges widely from 0.7% to 80.7%. Further studies with the support of long-term

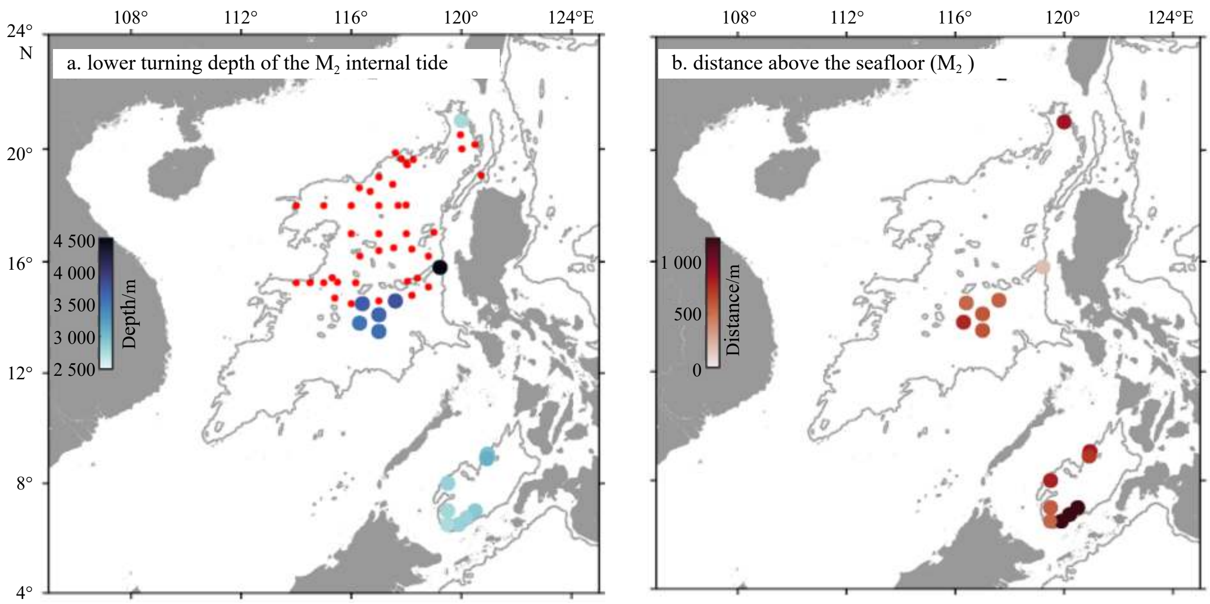

Fig. 5. Spatial distribution of the lower turning depths of the M_2 internal tide (a) and the distance between the turning points and the seafloor (b). The red dots indicate the stations where lower turning depths are not detected. The background gray contours indicate the 3 000 m isobath.

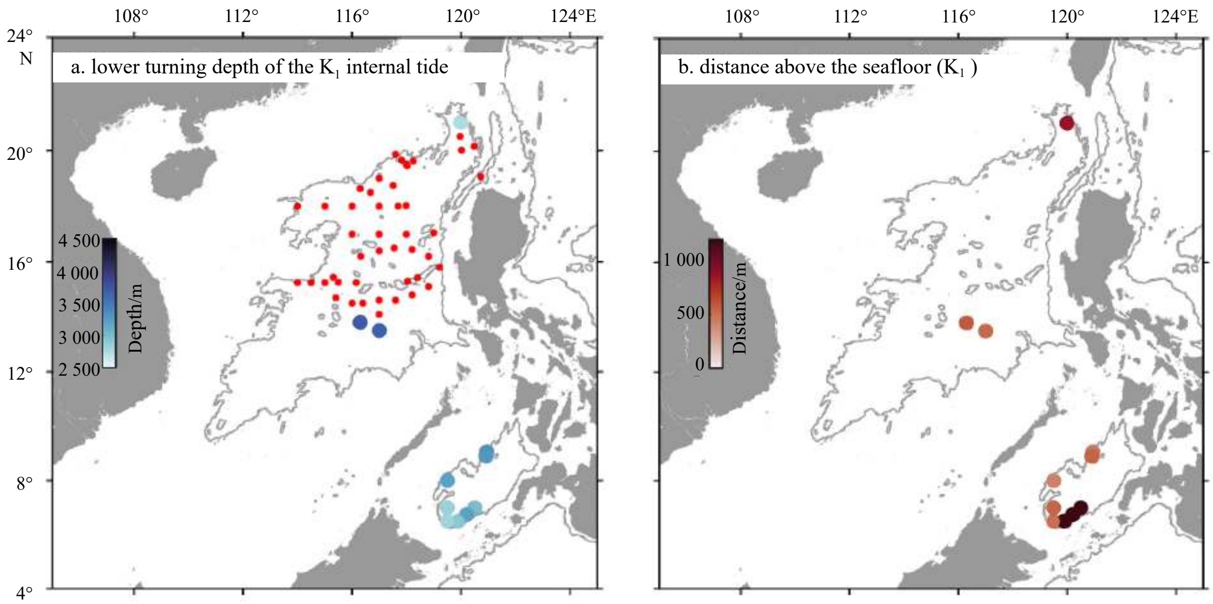

Fig. 6. Spatial distribution of the lower turning depths of the K_1 internal tide (a) and the distance between the turning points and the seafloor (b). The red dots indicate the stations where lower turning depths are not detected. The background gray contours indicate the 3 000 m isobath.

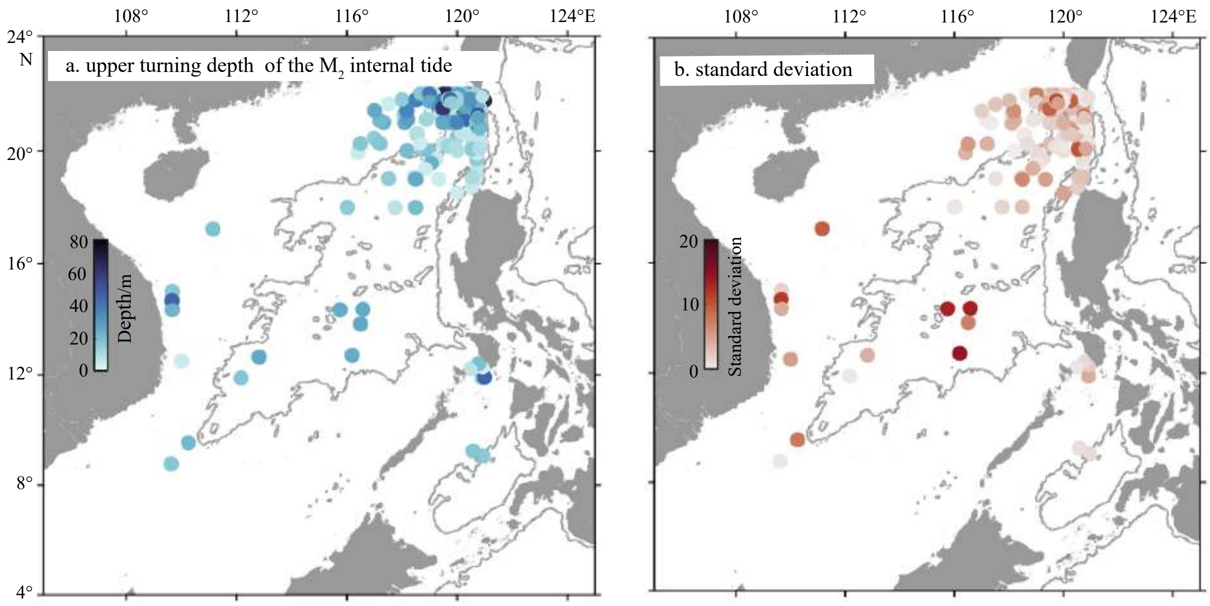

Fig. 7. Spatial distribution of the upper turning depths of the M_2 internal tide with the bin value of 5 m (a) and standard deviations of the calculated upper turning depths with different bin values of 2–8 m (b). The background gray contours indicate the 3 000 m isobath.

mooring data may be more convincing in understanding the uncertainties and temporal variations in the ITUTDs.

3.3 *Estimating turning depths with more than the traditional Coriolis approximation*

Considering their relatively shallow water depths, oceanic motions generally have very large horizontal scales, rendering the cosine terms of the Coriolis force insignificant such that they are typically neglected in traditional approximations. In the previous sections, turning depths were estimated based on the traditional Coriolis definition. However, when approaching a turning depth, the internal tidal beams are nearly perpendicular to the horizontal plane (Paoletti and Swinney, 2012); thus, the cosine term of the Coriolis force can no longer be neglected for motions with manifestly vertical characteristics (Gerkema et al., 2008). As the cosine terms of the Coriolis force act only in the zonal direction, the horizontal propagation direction of internal tides should be taken into account. For internal tides propagating at an angle d with respect to the east, the critical $N^2(z)$ can be derived following King et al. (2012):

$$N^2_{\rm crit} = \frac{\omega^2(f_s^2 + f_c^2 \sin d^2 - \omega^2)}{f_s^2 - \omega^2}, \tag{4}$$

where $f_s = 2\Omega \sin\varphi$ (in which Ω is the Earth's angular velocity and φ is the latitude in the northern hemisphere) and

$f_c = 2\Omega\cos\varphi$ are the sine and cosine terms of the Coriolis parameter, respectively. For zonally propagating internal tides, d equals zero (or 180°), and $N^2_{\text{crit}} = \omega^2$, which is the same as the traditional approximation.

The latitudinal dependence of the critical value of $N^2_{\text{crit}}/\omega^2$, considering the full Coriolis force and a given internal tide propagation direction, is shown in Fig. 8. For a fixed propagation direction, the discrepancy of the critical $N^2(z)$ value between the traditional approximation and the full definition increases poleward. The biggest difference occurs in the vicinity of the critical latitude (where the inertial frequency equals the tidal frequency, i.e., 74.5° for the M_2 constituent and 30° for the K_1 constituent). The SCS deep basin extends at relatively low latitudes from approximately 10°N to 20°N (the light gray areas in Figs 8a and b), but N^2_{crit} can still be significantly affected by the propagation direction. When internal tides propagate at a small angle relative to the zonal direction (less than the critical latitude), the discrepancy between the traditional approximation and the full definition increases with the angle (Figs 8a and b). By contrast, when the angle between the propagation direction and the zonal direction is greater than the critical latitude (the dark gray areas in Figs 8c and d), the N^2_{crit} term in Eq. (4) is always negative when it is equatorward of the critical latitude, and internal tides can propagate freely without any turning depth limitation. M_2 internal tides radiate from the Luzon Strait to the SCS along a stronger north-westward beam and a weaker south-westward beam (Zhao, 2014); the southwestward beam directs to the deep basin with an approximately fixed propagation direction of approximately 225° (a 45° angle relative to the zonal direction). The critical value of N^2_{crit} for M_2 internal tides under the full definition is approximately half of that under the traditional approximation, indicating a greater turning depth. K_1 internal tides radiate from the Luzon Strait to the SCS deep basin along one main beam with a propagation direction varying between approximately 190° and 240° (a 10°–60° angle relative to the zonal direction) under the effect of the Earth’s rotation (Zhao, 2014). The situation becomes slightly more complicated for the K_1 internal tide. During the first half of propagation (with a propagation direction from 190° to 210°), the discrepancy of the critical value of N^2_{crit} between the traditional approximation and the full definition increases significantly. Moreover, during the second half of propagation (with a propagation direction from 210° to 240°), K_1 internal tides are independent of the turning depths. These results are remarkably different from those under the traditional approximation. In addition, the critical latitudes can be shifted by several degrees under the impact of the background relative vorticity (Yang et al.,

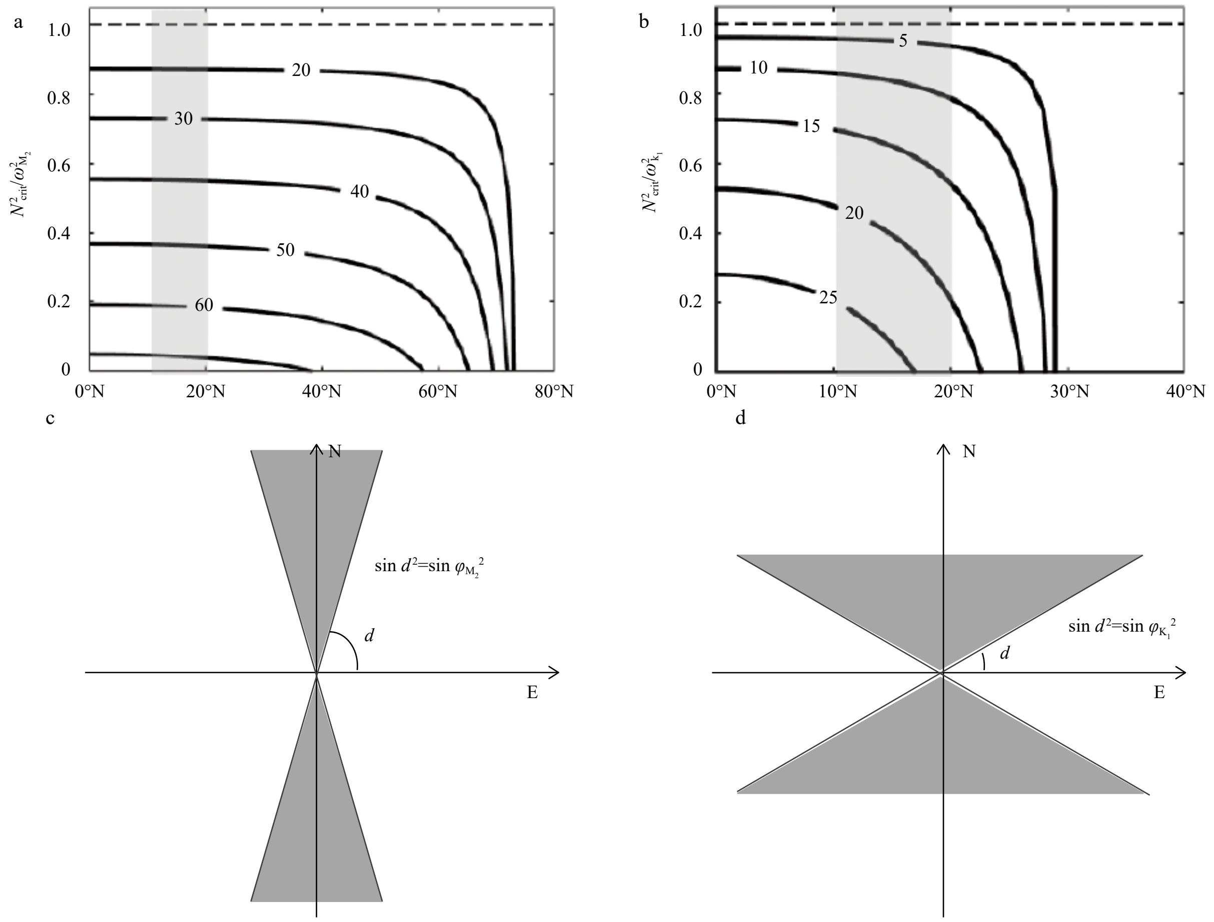

Fig. 8. Latitudinal dependence of the critical value of $N^2_{\text{crit}}/\omega^2$ with full consideration of the Coriolis force and a given internal tide propagation direction (angles in the zonal direction that are labeled on the isolines) for M_2 and K_1 tidal frequencies, respectively (a, b), and schematic diagram of the range of propagation directions when the propagation of internal tides is independent of the turning depth (dark gray patches) (c, d). The black dashed lines in a and b indicate the critical values under the traditional approximation, the light gray patches indicate the latitude range of the South China Sea deep basin. φ_{M_2} and φ_{K_1} are the critical latitudes for M_2 and K_1 internal tides, respectively.

2018), which suggests that an accurate prediction of the propagation of internal tides in the SCS is still very challenging.

4 Conclusions

This study introduced the concept of the upper turning depth in the context of internal tides and provide the first observational evidence for the existence of internal tide turning depths in the SCS based on both NSFS and WOD18 observations. The available data yielded a synoptic view of the spatial distribution of both ITLTDs and ITUTDs for M_2 and K_1 frequencies. The results suggest that ITLTDs exist at several abyssal stations in the SCS deep basin and can occur at depths greater than 1 000 m above the ocean bottom, indicating the possible existence of a broad abyssal internal wave evanescent region. ITLTDs were distributed mainly in the southern part of the basin, likely due to the greater water depths. ITUTDs are ubiquitous in the SCS and are generally tens of meters from the surface. ITUTDs are located mainly in the northeastern SCS, which is consistent with the intensive sampling there. However, the estimation of ITUTDs in this study has large uncertainties that are sensitive to the selected bin values. When the buoyancy frequencies are low enough to reach the tidal frequencies, ocean waters are very weakly stable. In contrast to the quiet abyssal ocean, the upper layer is stirred by winds and surface buoyancy fluxes, and the assumption that $N^2(z)$ profiles exhibit a monotonous decreasing trend from the pycnocline to the sea surface is not always valid.

The presence of turning depths can insulate propagating internal tidal beams from colliding with the air-sea interface and rough seafloor and thus may play important roles in the propagation and dissipation of internal tides in the SCS. In addition, internal tides generated beneath ITLTDs may be bottom trapped, as the wave energy decays exponentially from generation sites. That is, turning depths may affect the vertical energy dissipation profile of internal tides and thus impact the ocean state. It is necessary but challenging to quantitatively estimate the influence of turning depths on internal tide generation, propagation, and dissipation processes; this may require future modeling efforts.

Acknowledgements

Special gratitude goes to Wei Zhao and Chun Zhou (Ocean University of China) for collecting and generously providing the NSFC CTD data. We also thank the anonymous reviewers for their assistance in evaluating this paper.

References

Boyer T P, Baranova O K, Coleman C, et al. 2018. World Ocean database 2018. NOAA Atlas NESDIS 87. Silver Spring, MD, USA: NOAA

Broecker W S, Patzert W C, Toggweiler J R, et al. 1986. Hydrography, chemistry, and radioisotopes in the southeast Asian basins. Journal of Geophysical Research: Oceans, 91(C12): 14345–14354, doi: 10.1029/JC091iC12p14345

Carnes M R. 2009. Description and evaluation of GDEM-V3.0. Washington D.C.,USA: Nav. Res. Lab

Chen Yingying, Yu Kai, Dong Changming, et al. 2017. Evaluation of satellite-altimetry-derived pycnocline depth products in the South China Sea. Remote Sensing, 9(8): 822, doi: 10.3390/rs9080822

Dushaw B D, Sagen H. 2017. The role of simulated small-scale ocean variability in inverse computations for ocean acoustic tomography. The Journal of the Acoustical Society of America, 142(6): 3541, doi: 10.1121/1.5016816

Fang Huacan, Duan Menglan. 2014. Offshore Operation Facilities: Equipment and Procedures. Waltham, MA, USA: Elsevier, 807

Gerkema T, Lam F P A, Maas L R M. 2004. Internal tides in the Bay of Biscay: conversion rates and seasonal effects. Deep-Sea Research Part II: Topical Studies in Oceanography, 51(25–26): 2995–3008, doi: 10.1016/j.dsr2.2004.09.012

Gerkema T, Zimmerman J T F, Maas L R M, et al. 2008. Geophysical and astrophysical fluid dynamics beyond the traditional approximation. Reviews of Geophysics, 46(2): RG2004

Jan Sen, Chen C T A. 2009. Potential biogeochemical effects from vigorous internal tides generated in Luzon Strait: a case study at the southernmost coast of Taiwan. Journal of Geophysical Research Oceans, 114(C4): C04021, doi: 10.1029/2008JC004887

King B, Stone M, Zhang H P, et al. 2012. Buoyancy frequency profiles and internal semidiurnal tide turning depths in the oceans. Journal of Geophysical Research: Oceans, 117(C4): C04008, doi: 10.1029/2011JC007681

Li Yanan, Gao Zhanke, Suo Lili. 2013. Development in seawater salinity metrology: TEOS-10 and absolute salinity. Ocean Technology, 32(4): 118–123

Liang Jianjun, Li Xiaoming, Sha Jin, et al. 2019. The lifecycle of nonlinear internal waves in the northwestern South China Sea. Journal of Physical Oceanography, 49(8): 2133–2145, doi: 10.1175/JPO-D-18-0231.1

Lynn R J, Reid J L. 1968. Characteristics and circulation of deep and abyssal waters. Deep-Sea Research and Oceanographic Abstracts, 15(5): 577–598, doi: 10.1016/0011-7471(68)90064-8

Munk W H. 1981. Internal waves and small-scale processes. In Stommel H M, Warren B A, Wunsch C, eds. Evolution of Physical Oceanography: Scientific Surveys in Honor of Henry Stommel. Cambridge, UK: MIT Press, 264–291

Munk W, Wunsch C. 1998. Abyssal recipes II: energetics of tidal and wind mixing. Deep-Sea Research Part I: Oceanographic Research Papers. 45(12): 1977–2010, doi: 10.1016/S0967-0637(98)00070-3

Niwa Y, Hibiya T. 2011. Estimation of baroclinic tide energy available for deep ocean mixing based on three-dimensional global numerical simulations. Journal of Oceanography, 67(4): 493–502, doi: 10.1007/s10872-011-0052-1

Paoletti M S, Drake M, Swinney H L. 2014. Internal tide generation in nonuniformly stratified deep oceans. Journal of Geophysical Research: Oceans, 119(3): 1943–1956, doi: 10.1002/2013JC009469

Paoletti M S, Swinney H L. 2012. Propagating and evanescent internal waves in a deep ocean model. Journal of Fluid Mechanics, 706: 571–583, doi: 10.1017/jfm.2012.284

Qu Tangdong, Girton J B, Whitehead J A. 2006. Deepwater overflow through Luzon Strait. Journal of Geophysical Research: Oceans, 111(C1): C01002, doi: 10.1029/2005JC003139

Van Haren H, Millot C. 2006. Determination of buoyancy frequency in weakly stable waters. Journal of Geophysical Research: Oceans, 111(C3): C03014, doi: 10.1029/2005JC003065

Yang Wei, Hibiya T, Tanaka Y, et al. 2018. Modification of parametric subharmonic instability in the presence of background geostrophic currents. Geophysical Research Letters, 45(23): 12957–12962, doi: 10.1029/2018GL080183

Zhao Zhongxiang. 2014. Internal tide radiation from the Luzon Strait. Journal of Geophysical Research: Oceans, 119(8): 5434–5448, doi: 10.1002/2014JC010014